Label-free electrochemical impedance detection of kinase and phosphatase activities using carbon nanofiber nanoelectrode arrays

Yifen Li, Lateef Syed, Jianwei Liu, Duy H. Hua, Jun Li

Published Version Information

Citation: Li, Y., Syed, L., Liu, J., Hua, D. H., & Li, J. (2012). Label-free electrochemical impedance detection of kinase and phosphatase activities using carbon nanofiber nanoelectrode arrays. Analytica Chimica Acta, 744, 45-53.

Digital Object Identifier (DOI): doi:10.1016/j.aca.2012.07.027

Publisher's Link: http://www.sciencedirect.com/science/article/pii/S0003267012010574

Label-free electrochemical impedance detection of kinase and phosphatase activities using carbon nanofiber nanoelectrode arrays

Yifen Li[1], Lateef Syed[1], Jianwei Liu[1], Duy H. Hua[1], Jun Li[1,*]

[1]Department of Chemistry, Kansas State University, Manhattan, KS 66506, USA

Abstract

We demonstrate the feasibility of a label-free electrochemical method to detect the kinetics of phosphorylation and dephosphorylation of surface-attached peptides catalyzed by kinase and phosphatase, respectively. The peptides with a sequence specific to c-Src tyrosine kinase and protein tyrosine phosphatase 1B (PTP1B) were first validated with ELISA-based protein tyrosine kinase assay and then functionalized at vertically aligned carbon nanofiber (VACNF) nanoelectrode arrays (NEAs). Real-time electrochemical impedance spectroscopy (REIS) measurements showed reversible impedance changes upon addition of c-Src kinase and PTP1B phosphatase. Only small and unreliable impedance variation was observed during the peptide phosphorylation, but a large and fast impedance decrease was observed during the peptide dephosphorylation at a series of PTP1B concentrations. The REIS data of dephosphorylation displayed a well-defined exponential decay following the Michaelis-Menten heterogeneous enzymatic model with a consistent specific constant $k_{cat}/K_m = (2.13\pm0.09)x10^7$ $M^{-1}s^{-1}$. This electrochemical method can be potentially used as a label-free method for profiling enzyme activities in fast reactions.

Keywords:

real-time electrochemical impedance spectroscopy

phosphorylation

dephosphorylation

heterogeneous enzyme kinetics

vertically aligned carbon nanofibers

nanoelectrode array

c-Src tyrosine kinase

protein tyrosine phosphatase 1B

Abbreviations: real-time electrochemical impedance measurements (REIS), nanoelectrode array (NEA), vertically aligned carbon nanofiber (VACNF), protein tyrosine phosphatase 1B (PTP1B), APTES, sulfo-NHS, sulfo-EMCS, HRP, CNF, FESEM, ELISA, EGFR

* Corresponding author at: Department of Chemistry, Kansas State University, Manhattan, KS 66506, USA. Tel.: +1 785 532 0955; fax: +1 785 532 6666.

E-mail address: junli@k-state.edu (J. Li).

1. Introduction

Protein kinases and phosphatases have been under intense study for their roles in fundamental biochemical processes and signal transduction pathways [1, 2]. Recently, they have become attractive targets for therapeutic drug discovery [3-6]. Kinase catalyzes the transfer of the phosphate group at γ-position of ATP to specific protein/peptide substrates; this process is referred to as phosphorylation. Phosphatase catalyzes the reverse process, removing the phosphate group from the phosphorylated substrates; this process is called dephosphorylation. Phosphorylation and dephosphorylation are reversible dynamic processes, which are important regulatory mechanisms in both prokaryotic and eukaryotic organisms [7].

The most direct way of detecting phosphorylation is to measure the radioactive ^{32}P transferred from γ-^{32}P-ATP to the amino acid residues on the protein substrates [7-9]. Other major methods include fluorescence labeling, chemiluminescence, electroluminescence [10-15], mass spectroscopy [16, 17], and

surface plasmon resonance [18-22]. Recently, electrochemical detections of kinase activities have been reported using redox-labeled cosubstrate adenosine 5'-[γ-ferrocene] triphosphate (Fc-ATP) [23] or binding of gold nanoparticles to thiol-modified adenosine 5'-[γ-thio] triphosphate (ATP-S) [24]. These methods either require costly reagent (chemically labeled ATP or phosphor-specific antibodies) or are limited by the lack of miniaturization and/or multiplexing capability. In this study, we explore the feasibility of a label-free rapid electrochemical method which could be implemented on a multiplex chip. Reversible phosphorylation and dephosphorylation under the heterogeneous catalyses of protein tyrosine kinase c-Src and protein tyrosine phosphatase 1B (PTP1B), respectively, have been detected and quantified.

C-Src kinase is a cytoplasmic protein belonging to a family of non-receptor protein tyrosine kinases that catalyze the phosphorylation to specific tyrosine residues of the substrates. In normal cells, c-Src kinase participates in proliferation, maintenance of normal intercellular contacts, and cell motility [25]. Clinical studies have shown that increased activity of c-Src kinase is correlated to cancer progression. Also, high expression levels of c-Src kinase are found in human tumors corresponding to lung, breast, pancreatic, colon, and prostate cancers [26]. Small inhibitors against c-Src kinase have been developed as anti-cancer drugs [27]. PTP1B is a non-transmembrane protein that dephosphorylates phosphotyrosine residues on protein substrates. It is known to inhibit insulin and leptin signaling, and has been an attractive therapeutic target for diabetes, obesity [28], and anti-tumor drugs [29, 30].

The label-free electrochemical method is illustrated in Fig. 1 in which peptides are immobilized on an electrode surface. Phosphorylation of the peptides by kinase introduces phosphate groups and negative charges to the electrode surface. Reversely, dephosphorylation of the phosphorylated substrates by phosphatase removes the negatively charged phosphate groups from the peptides. The changes in charge density and/or conformation of the peptides accompanying these reactions may induce changes in electrochemical impedance |Z|. This method may be applied on multiplex electrode arrays on a microchip enabling simultaneously profiling of the activities of multiple kinases and phosphatases.

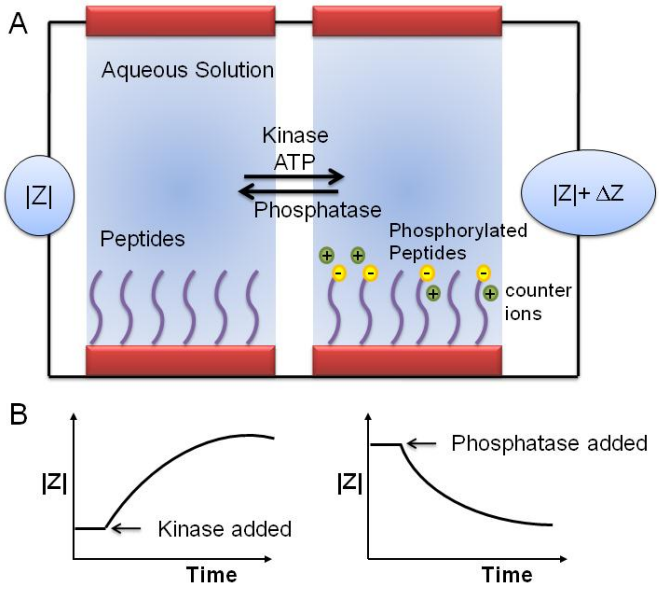

Fig. 1. Schematic of the principles of label-free electrochemical impedance detection of enzymatic activities of kinase and phosphatase. (A) The reversible phosphorylation and dephosphorylation of surface-attached peptide substrates catalyzed by kinase and phosphatase, respectively. (B) Schematic of real-time electrochemical impedance spectroscopy (|Z| vs. time) during the enzymatic phosphorylation and dephosphorylation reactions.

Particularly, we apply this method on a nanoelectrode array (NEA) fabricated with vertically aligned carbon nanofibers (VACNFs) in SiO_2 matrix with only the very end exposed [31, 32]. As demonstrated in previous studies [31, 32], the carbon nanofiber (CNF) tip can be covalently attached with biomolecules. The electrochemical properties of the VACNF NEAs are highly sensitive to the structure of the biomolecules at the highly miniaturized electrode surface. Conceptually, phosphorylation and dephosphorylation of the peptide substrates attached to the VACNF NEA could affect the molecular packing and generate notable impedance changes. However, the kinetic study of the heterogeneous enzymatic reaction at NEAs has not been reported. Here we demonstrate that the reversible impedance changes associated with phosphorylation and dephosphorylation of the peptides covalently attached to the VACNF NEA can be detected with label-free real-time impedance spectroscopy (REIS). The impedance

change was found to strongly depend on enzyme's specificity constant. The rate of dephosphorylation catalyzed by PTP1B was found much higher than that of c-Src phosphorylation to the same peptide substrate attached at the VACNF NEA. The PTP1B dephosphorylation process showed a well-defined kinetic curve, which can be quantitatively analyzed with a heterogeneous Michaelis-Menten enzymatic model.

2. Materials and methods

2.1 Materials

Tyrosine kinase buffer (500 mM HEPES, pH 7.4, 200 mM $MgCl_2$, 1 mM $MnCl_2$, and 2 mM Na_3VO_4) was purchased from Sigma-Aldrich (Saint Louis, Missouri). Active c-Src kinase protein (N-terminal 6His-tagged recombinant human c-Src, molecular weight 61.7 kDa) was purchased from Milipore (Billerica, MA). Peptide substrate of c-Src kinase (Biotin-AEEEIYGEFEAKKKKC) was synthesized by AnaSpec, Inc. (Fremont, CA). The Protein Tyrosine Kinase Assay Kit of an enzyme-linked immunosorbent assay (ELISA), including adenosine-5'-triphosphate (ATP), epidermal growth factor receptor (glycosylated EGFR, molecular weight 170 kDa) and monoclonal anti-phosphotyrosine-peroxidase conjugate was purchased from Sigma-Aldrich (Saint Louis, Missouri). PTP1B (residues 1-322, molecular weight 37.4 kDa) and phosphatase buffer (50 mM HEPES, pH 7.2, 1 mM EDTA, 1 mM DTT, and 0.05% NP-40) were purchased from Enzo Life Sciences, Inc. (Plymouth Meeting, PA). Chemicals (3-aminopropyl)triethoxysilane (APTES), 2-[2-(2-methoxyethoxy)ethoxy]acetic acid, *N*-ethyl-*N*′-(3-dimethylaminopropyl)carbodiimide hydrochloride (EDC), hydroxy-2,5-dioxopyrrolidine-3-sulfonic acid sodium salt (sulfo-NHS), 9-fluorenylmethyl *N*-(6-aminohexyl) carbamate hydrobromide, and piperidine were purchased from Sigma-Aldrich. *N*-[ε-Maleimidocaproyloxy]sulfosuccinimide ester (sulfo-EMCS) was purchased from Thermo Fisher Scientific Inc. (Waltham, MA). Carboxylated latex beads derivatized with streptavidin and impregnated with yellow-green fluorescent dyes (in wt 1%

suspension, average diameter of 50 nm, with excitation wavelength at 470 nm and emission wavelength at 505 nm) were purchased from Sigma-Aldrich (Saint Louis, Missouri).

2.2 Fabrication of VACNF NEAs

The NEAs were fabricated by encapsulating VACNFs in a SiO_2 matrix on a silicon chip using the method described in the previous papers [31, 32]. Briefly, VACNFs of the average length of ~5 μm were grown on Cr-coated Si substrate using a DC-biased plasma enhanced chemical vapor deposition (PECVD). A thin nickel film of ~22 nm was used as a catalyst to promote carbon nanofiber (CNF) growth. The electric field helped to align the CNF vertically on the substrate surface. Dielectric SiO_2 was deposited using chemical vapor deposition (CVD) from vapor-phase precursor tetraethylorthosilicate (TEOS) to fully encapsulate the bottom Cr metal contact layer and each individual CNFs. Mechanical polishing was applied using 0.3 μm alumina slurry to produce a flat surface. Reactive ion etching (RIE) with a mixture of CHF_3 and O_2 gases was then performed to selectively etch away desired amount of SiO_2 and expose some of the CNF tips. A typical VACNF NEA for electrochemical measurements consists of randomly distributed CNF tips with an average CNF diameter of ~200 - 300 nm and an average spacing over ~1 μm (~1 - 10 x 10^6 CNFs/cm^2), as shown in Fig. S1 (Supplementary Information). A length of ~50 - 300 nm at the CNF tips were exposed at the SiO_2 surface, which can be controlled by varying the RIE time to selectively remove SiO_2.

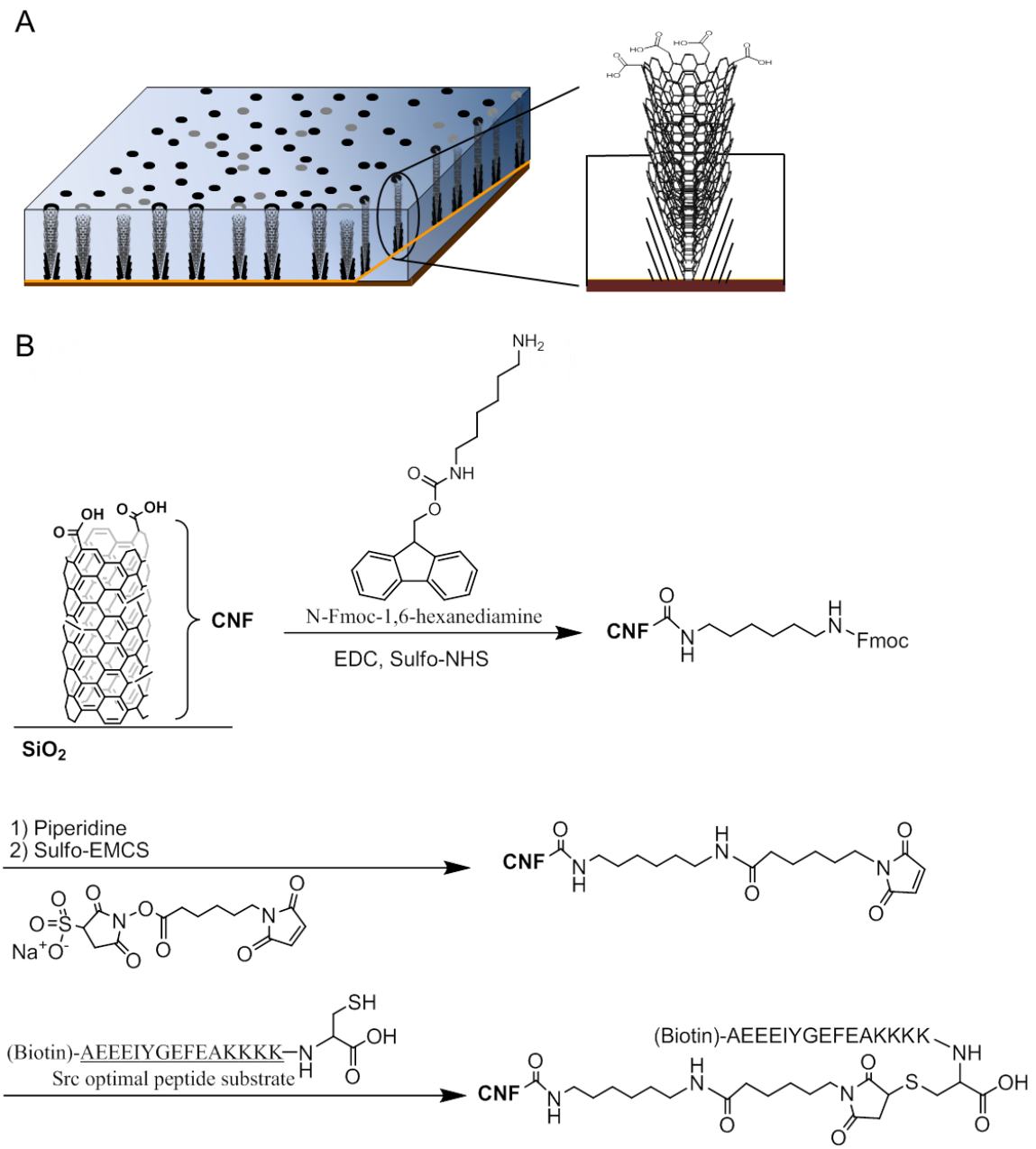

Fig. 2. The scheme for functionalizing peptide to CNF tips. (A) Schematic drawing of VACNFs embedded in SiO_2 matrix; (B) a biotinylated peptide substrate specific to c-Src kinase is covalently attached to the CNF tip through coupling the thiol group in the cysteine residue with a maleimide group of a linker molecule.

2.3 Electrode pre-conditioning

Before each use, VACNF NEAs were further polished with 0.05 μm γ-alumina slurry (Buehler) on napless polishing cloth for 5 min, followed by rinsing with deionized water. The polishing and rinsing procedures were repeated once followed by sonication in deionized water for 15 min. The VACNF NEAs were then electrochemically activated by etching in 1.0 M NaOH solution using four cycles of cyclic voltammetry (CV) with a potential range of -0.10 V to 1.20 V (vs. Ag/AgCl (3 M KCl)) at a scan rate of 50 $mV \cdot s^{-1}$. Electrodes were rinsed with deionized water and stored in a Petri dish before use.

2.4 Functionalization and passivation of the VACNF NEA chip

To reduce nonspecific adsorption, the SiO_2 surface of VACNF NEAs was first passivated with protective moieties containing ethylene glycol, as described in our previous report [33, 34]. The chip was immersed in an 8 g L^{-1} solution of APTES in ethanol for 20 min to produce a primary amine derivatized surface. The chip was treated with 50 μL solution of 0.1 mM of 2-[2-(2-methoxyethoxy)ethoxy]acetic acid, 100 g L^{-1} of EDC, and 50 g L^{-1} of sulfo-NHS, and incubated at room temperature for 2 hours. The carboxylic acid group of 2-[2-(2-methoxyethoxy)ethoxy]acetic acid formed an amide bond with the amino function on the chip surface, leaving ethylene glycol moiety covering the surface. The molecules at the CNF tips were then removed by electrochemical etching at 1.2 V (vs. Ag/AgCl (3 M KCl)) for 20 sec. in 1.0 M NaOH solution. This process regenerated clean CNF tips which contain abundant carboxylic acid functional groups.

The scheme for functionalization of the peptide to a CNF tip is illustrated in Fig. 2. A cysteine was added to the carboxyl terminus of the original c-Src kinase peptide substrate (AEEEIYGEFEAKKKK), so that the thiol group of the cysteine can be conjugated to the CNF through a maleimide linker. In addition, a biotin was added to the *N*-terminus for the binding study described below. A 50 μL solution of 0.1 mM *N*-Fmoc-1,6-diaminohexane hydrobromide, 100 g L^{-1} of EDC, and 50 g L^{-1}

of sulfo-NHS were applied to the chip and incubated at room temperature for 2 hours. The unprotected amine function of the diaminohexane was coupled with the carboxylic acid group of CNF. The Fmoc protecting group was then removed by incubating in 10% piperidine in DMF at room temperature for 15 min followed by rinsing with DMF. The deprotection procedure was repeated once followed by rinsing with deionized water. A 1.0 mM sulfo-EMCS linker was then applied to the chip and incubated at room temperature for 30 min, allowing the deprotected amine group to react with sulfo-EMCS. Then 50 μL solution of 2 μM biotinylated c-Src peptide substrate with the cysteine at C-terminus (i.e. biotin-AEEEIYGEFEAKKKKC) was applied to the chip and incubated at room temperature for 2 hours. Hence, the peptide substrate was immobilized on the chip through the Michael addition reaction between the thiol group of cysteine residue and the maleimide moiety of CNFs.

To verify the coupling of the peptides to CNFs, streptavidin-derivatized latex beads (50 nm in diameter) in phosphate buffered saline solution (PBS, pH 7.4) with 0.005% Tween 20 were applied to the chip followed by extensive washing. The impregnated yellow-green fluorescent dyes in the beads were revealed under a fluorescence optical microscope (Axioskop II, Carl Zeiss) as shown in Fig. S2 (Supplementary Information). The attachment of the beads at the CNF tips through the specific biotin-streptavidin binding was further verified with a field-emission scanning electron microscope (FESEM) (Leo 1550, Zeiss) as shown in Fig. 3.

2.5 ELISA assays to validate the activities of c-Src kinase and PTP1B

The detailed protocols for ELISA-based protein tyrosine kinase assay using a commercial kit are illustrated in Fig. S3. The peptide substrates at a concentration of 0.125 $mg \cdot mL^{-1}$ in PBS were added to wells of a 96-well plate, and incubated overnight at 37 ºC. The peptide solution was then removed and the plate was dried at 37 ºC for 2 hours. A volume of 110 μL tyrosine kinase buffer (with the composition given in "2.1 *Materials*") containing active c-Src kinase and ATP was added to each well for reactions. C-

Src kinase concentration in the mixed solution was varied from 0.18 nM to 5.9 nM (corresponding to 1.25 – 40 ng of c-Src in 110 μL of solution) and the ATP concentration was fixed at 0.30 mM. After incubation and washing, a solution of phosphotyrosine monoclonal antibody linked with horseradish peroxidase (HRP) was applied to specifically bind with phosphotyrosine residues of the peptide substrates. HRP then catalyzed the conversion of supplied colorless *o*-phenylenediamine (OPD) into brown-color 2,3-diaminophenazine (DAP) which presents a peak absorbance at 490 nm. The absorbance at 490 nm in each well was read by a microplate reader (model EL307C, BioTek).

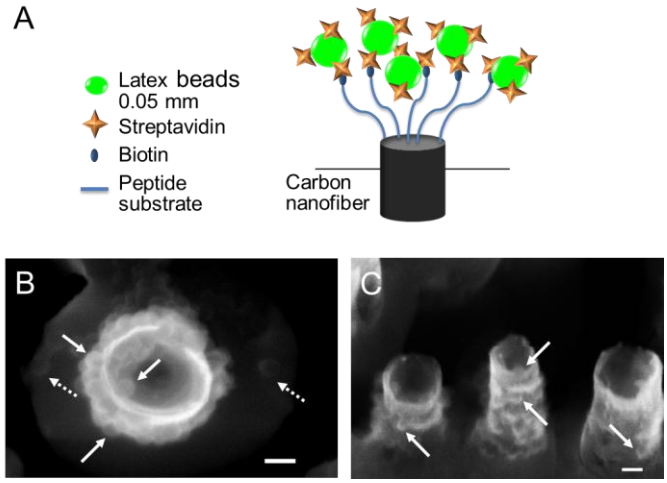

Fig. 3. Verification of the coupling of the peptide and CNF using streptavidin-labeled fluorescent beads. (A) A schematic drawing shows fluorescent beads selectively bound to the surface-functionalized peptide through biotin-streptavidin interaction; (B and C): FESEM images at top and 45° perspective views show that many 50-nm diameter beads were attached to the exposed CNF tips (indicated by solid arrows) while only a few beads nonspecifically bound to the SiO_2 surface (as indicated by dashed arrows). The scale bars in B and C are 100 nm.

The dephosphorylation activity of PTP1B was validated by measuring the amount of remaining phosphotyrosine after incubation using the same ELISA assay kit. The 96-well plate was first coated with the biotinylated peptide substrates. The solution of 5.9 nM c-Src kinase and 0.3 mM ATP in tyrosine

kinase buffer was added to each well and incubated at room temperature for one hour to ensure that tyrosine residues on all peptides were phosphorylated. After washing with PBS-Tween 20 buffer and drying for 2 hours at 37 °C, PTP1B in 110 μL phosphatase buffer was added to the well and incubated at room temperature for 30 min. for dephosphorylation. The PTP1B concentration was varied from 0.076 nM to 2.4 nM. In some experiments, the phosphatase buffer was modified by removing the detergent NP-40 to get more reliable electrochemical measurements. The wells were washed thoroughly with PBS-Tween 20 buffer and dried. Then a similar ELISA procedure as described above was applied. The absorbance at 490 nm, which indicates the amount of remaining phosphotyrosine in each well, was read with the BioTek microplate reader.

2.6 Electrochemical measurements

All electrochemical measurements were performed in a TEFLON cell with a total volume of ~120 μL sealed against the VACNF NEA chip with a 3-mm i.d. O-ring. The experiment was controlled by a potentiostat (PARSTAT 2273, Princeton Applied Research Corporation) using a three-electrode setup (working electrode: VACNF NEA; counter electrode: a coiled platinum wire; and quasi-reference electrode: an Ag wire). The real-time electrochemical impedance spectroscopy (REIS) was performed at the open circuit potential with a 20 mV rms AC voltage at fixed frequency of 1000 Hz.

3. Results and Discussion

3.1 Characterization of peptide functionalization at CNF tips

Functionalization of the peptide to the carboxylic groups at the CNF tip involves three steps illustrated in Fig. 2B. A biotinylated peptide substrate specific to c-Src kinase was covalently attached to

CNFs through coupling of the thiol group of the cysteine residue in the peptide with the maleimide group at the end of the linker molecule. The major part of the peptide sequence (i.e. AEEEIYGEFEAKKK, the optimal peptide substrate for c-Src kinase) was selected by screening a combinatorial peptide library and reported to undergo *in vitro* phosphorylation by c-Src kinase with very high efficiency [35]. As illustrated in Fig. 3A, a biotin was added to the distal end (i.e. *N*-terminus) of the peptide substrate in order to verify its functionalization to the exposed CNF tip through specific binding with streptavidin-derivatized fluorescent latex beads. Clear isolated fluorescent spots were observed under an optical microscope as shown in Fig. S2, attributed to the clusters of latex beads attached to CNF tips. In addition, FESEM images in Figs. 3B and 3C directly showed that many beads with ~50 nm diameter were attached to the exposed CNF tips (indicated by solid arrows), while only a few beads bound to the SiO_2 surface (indicated by dashed arrows). Due to charging effects, it was difficult to obtain FESEM images of nonconductive latex beads at higher resolution. For better graphical presentation, images taken from CNFs with the diameter larger than the average were shown. Interestingly, the beads bind not only to the very end of the tip but also to the exposed sidewalls. This is consistent with the presence of many broken graphitic edges along the sidewall as a result of the unique microstructure of CNFs, which consists of a stack of conical graphitic structures as illustrated in Fig. 2A, instead of concentric seamless tubes [36]. It is convincing that peptide substrates are covalently attached to the CNF tip.

3.2 Validation of the enzymatic activities using the ELISA assay

First, an ELISA assay using the commercial Protein Tyrosine Kinase Assay Kit was adapted to validate the enzymatic activity of c-Src kinase on the designed biotinylated peptide substrate. The detailed procedure is illustrated in Fig. S3. The absorbance at 490 nm was plotted vs. the quantity of kinase in Fig. 4A. Clearly, the concentration of produced phosphotyrosine was proportional to that of c-Src kinase in the range from 0.18 nM to 5.9 nM (1.25 - 40 ng in 110 μL of solution). There was no difference in absorbance for the peptide substrate with and without biotin (not shown), which confirms that

biotinylation does not affect the properties of the peptide. A negative control experiment was performed using another kinase, Epidermal Growth Factor Receptor (EGFR), which showed very low absorbance (data not shown). These studies validated that the designed peptide substrate (i.e. biotin-AEEEIYGEFEAKKKC) is highly specific to c-Src kinase.

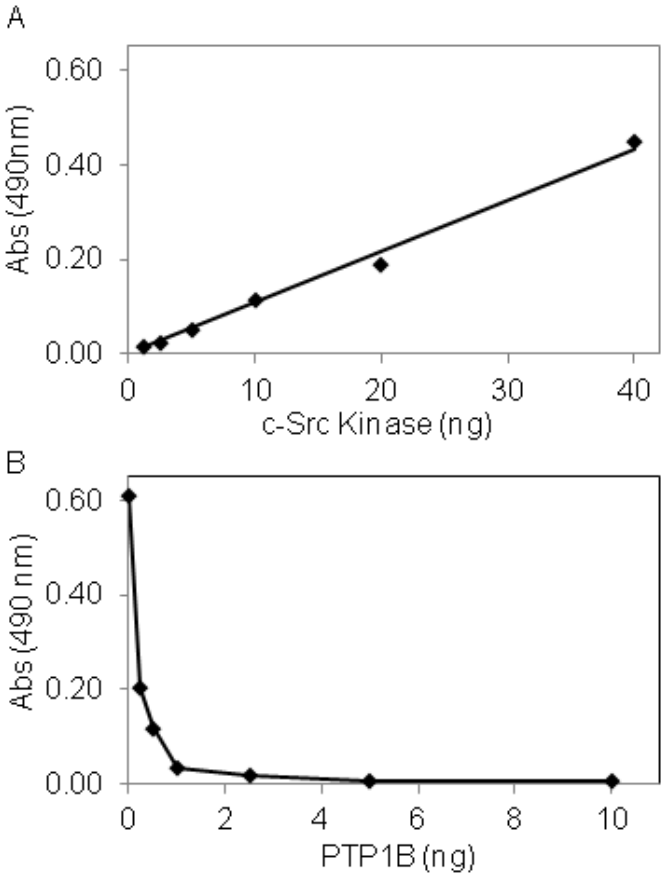

Fig. 4. Validation of enzymatic activity with ELISA assay. (A) Phosphorylation of the biotinylated peptide (biotin-AEEEIYGEFEAKKKC) by c-Src kinase measured with an ELISA assay following the procedure described in Fig. S3. The absorbance at 490 nm reflects the amount of phosphotyrosine, which is clearly proportional to the concentration of c-Src kinase from 0.18 nM to 5.9 nM (i.e. 1.25 - 40 ng in 110 μL solution). The concentration of ATP in all reactions was fixed at 0.30 mM. (B) Dephosphorylation by PTP1B phosphatase measured with the same ELISA assay. The tyrosine residue in the biotinylated peptide was first phosphorylated by prolonged incubation in 5.9 nM c-Src kinase. PTP1B at concentrations from 0.076 nM to 2.4 nM (i.e. 0.31 - 10 ng in 110 μL solution) were

then added to remove the phosphate group from phosphotyrosine, and caused a decrease in the absorbance at 490 nm.

The activity of PTP1B on the same biotinylated peptide substrates was also validated with the same ELISA assay. The peptide coated in the wellplate was first incubated in a solution of 5.9 nM c-Src kinase and 0.3 mM ATP at room temperature for one hour to ensure that all tyrosine residues on the peptides were phosphorylated. After washing and drying, solutions containing 0.31 – 10 ng of PTP1B in 110 μL phosphatase buffer (i.e. 0.076 nM to 2.4 nM) were added to the wells and incubated at room temperature for 30 min and then followed by a similar ELISA procedure as above. The absorbance at 490 nm was plotted in Fig. 4B vs. the quantity of PTP1B. The absorbance, which is proportional to the concentration of remaining phosphotyrosine, dropped from ~0.60 to 0.12 with only 0.5 ng (0.12 nM) PTP1B. In the kinase measurements, the absorbance only increased by 0.45 even at the highest c-Src kinase concentration (5.9 nM). Clearly, the catalytic efficiency of PTP1B is higher than that of c-Src kinase.

3.3 Real-time electrochemical impedance (REIS) measurements

Generally, there are two mechanisms for the electrochemical impedance measurements. The more common one employs redox mediators, such as an equimolar mixture of $[Fe(CN)_6]^{3-}/[Fe(CN)_6]^{4-}$ couple, to probe Faradaic impedance associated with the electron transfer resistance R_{ct} in the equivalent circuit. The changes in the film thickness and packing density will affect the accessibility of the redox mediators to the electrode surface and the amplitude of R_{ct} [37]. In the other mechanism, capacitive currents are measured without using redox species. These currents are mainly due to charging/discharging the electrical double layer at the electrolyte-electrode interface (i.e. C_{dl} in the equivalent circuit), which are also sensitive to the film packing and charge density on the electrode surface.

However, we found that the mediator mechanism was not applicable in this study. The activity of c-Src kinase was significantly suppressed when 1.0 mM of redox couple $[Fe(CN)_6]^{3-}/[Fe(CN)_6]^{4-}$ was added, as shown in the ELISA measurements in Fig. S4. As a result, our electrochemical impedance measurements were performed using the mediator-free mechanism. The detergent NP-40 in the commercial phosphatase buffer solution was also found not suitable for electrochemical measurements since it tended to induce bubbles at the electrode surface, leading to large noises. Thus the buffer composition for electrochemical measurements was modified and validated with the ELISA as shown in Figs. S4 and S5. The phosphorylation and dephosphorylation reactions only took a few minutes, which can be captured by REIS at a fixed frequency of 1000 Hz.

Fig. 5 shows the REIS of a peptide-functionalized VACNF NEA upon adding 20 μL c-Src kinase or PTP1B phosphatase, respectively, into 90 μL of corresponding buffer solutions. Only small a change (<0.5%) in the total impedance value |Z| was observed with the final c-Src kinase concentration as high as 5.9 nM. The change was superimposed on the step-like jump due to disturbance to the solution, as shown in Fig. 5A. The impedance change was slow and unreliable. After the peptide at the VACNF NEA was fully phosphorylated after 1-hour incubation, the buffer was replaced with 90 μL modified phosphatase buffer. The dephosphorylation reaction was monitored with REIS as shown in Fig. 5B. A stable |Z| at ~18,175 Ω was observed at the beginning. A sharp decrease in |Z| by ~1,150 Ω (~6.3%) was observed over the ~100 s period after adding 20 μL PTP1B (to the final concentration of 2.4 nM). The experiments were repeated, and the results indicated that the peptide attached to the VACNF NEA could be reversibly phosphorylated and dephosphorylated by switching the enzymes and corresponding buffers. The impedance change corresponding to the dephosphorylation by PTP1B was consistently larger than that of the phosphorylation by c-Src kinase. This was likely due to the difference in the enzyme activities. Consistent with the ELISA assay, the REIS measurements for negative control using EGFR did not show clear kinetic profiles.

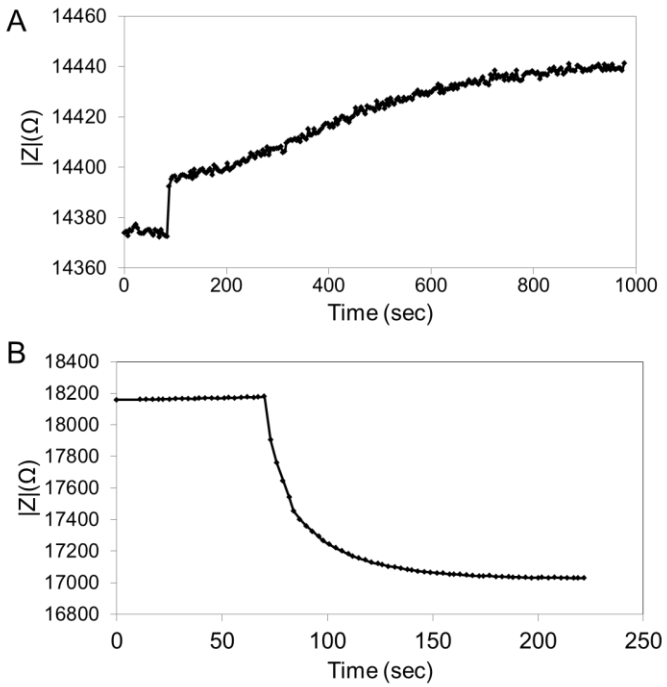

Fig. 5. Real-time electrochemical impedance measurements (|Z| vs. time) of peptide-functionalized VACNF NEAs. (A) Upon addition of 20 μL c-Src kinase (at 100 second) to 90 μL kinase buffer (i.e. 5.9 nM kinase and 0.30 mM ATP in the final solution), and (B) upon addition of 20 μL PTP1B (at 73 second) to 90 μL phosphatase buffer (2.4 nM final concentration). The impedance value |Z| varied slowly after c-Src kinase was added, but decreased rapidly after PTP1B was added.

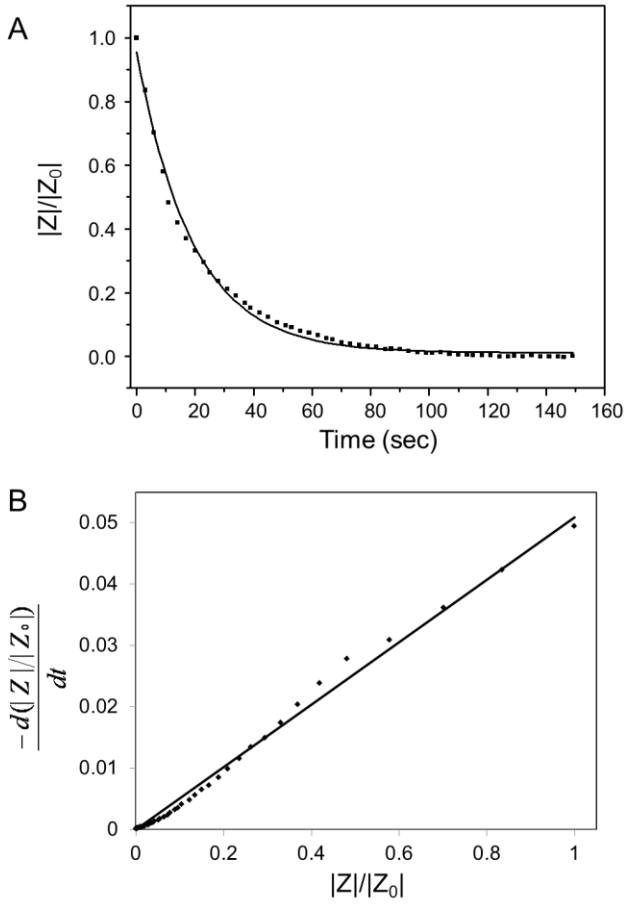

Fig. 6. Analyses of the enzymatic kinetics of the dephosphorylation process. (A) The real-time impedance data (as shown in Fig. 5B) at a peptide-functionalized VACNF NEA after adding 2.4 nM PTP1B (10.0 ng in 110 μL solution) was normalized and fit with an exponential function $|Z|/|Z_0| = 0.944 \cdot \exp(-t/19.1)$. (B) The plot of $-d(|Z||Z_0|)/dt$ vs. $|Z|/|Z_0|$ fit by a straight line with a slope of 0.0522 s^{-1}.

3.4 Enzyme kinetics analysis

The fast kinetics and the notable impedance change during dephosphorylation by PTP1B made it possible for quantitative analysis of enzyme activity based on the REIS results. The raw REIS data in Fig. 5B after addition of PTP1B was extracted and modified in three steps: (1) a linear baseline drift (almost a

constant at ~17,000 Ω) was subtracted; (2) the subtracted |Z| value was normalized to $|Z_0|$, the value right before adding PTP1B; and (3) the time at PTP1B addition was reset to zero. The modified curve (Fig. 6A) was then nicely fit with an exponential decay with $|Z|/|Z_0| = 0.944 \cdot \exp(-t/19.1)$. This kinetic data can be well described by a heterogeneous enzymatic model modified from Michaelis-Menten kinetics [38] as below:

$$E + S_s \underset{k_{-1}}{\overset{k_1}{\rightleftharpoons}} ES_s \xrightarrow{k_{cat}} E + P_s + P \quad (1)$$

where E, S_s, ES_s, P_s and P represent the enzyme (PTP1B), the surface-bound phosphorylated peptide substrate, the enzyme-substrate complex on the electrode surface, the product of dephosphorylated peptide substrate on the electrode surface, and the product of cleaved phosphate, respectively. The reaction rate can be defined as

$$\upsilon = -\frac{d\Gamma_{Ss}}{dt} = \frac{d\Gamma_{Ps}}{dt} = \frac{k_{cat}[E_0] \times \Gamma_{Ss}}{K_m + [E_0]} \quad (2)$$

where k_{cat} is the dissociation rate constant, $K_m = (k_{cat}+k_{-1})/k_1$ is the Michaelis-Menten constant, and Γ_{Ss}, Γ_{Ps} represent the surface densities of phosphorylated and dephosphorylated peptide substrates, respectively. At low enzyme concentrations where $[E_0] << K_m$, an approximate relationship can be obtained as

$$\upsilon = -\frac{d\Gamma_{Ss}}{dt} = \frac{d\Gamma_{Ps}}{dt} = \frac{k_{cat}}{K_m}[E_0] \times \Gamma_{Ss} \quad (3)$$

The reaction rate υ (or $-d\Gamma_{Ss}/dt$) is proportional to the normalized impedance change $-d(|Z|/|Z_0|)/dt$ and the surface density of phosphorylated substrate Γ_{Ss} is also proportional to $|Z|/|Z_0|$ with the same coefficient. As a result, the slope of $-d\Gamma_{Ss}/dt$ vs. Γ_{Ss} is the same as that of $-d(|Z|/|Z_0|)/dt$ vs. $|Z|/|Z_0|$, and is equal to $(k_{cat}/K_m)[E_0]$, namely

$$-\frac{d\Gamma_{Ss}/dt}{\Gamma_{Ss}} = -\frac{d(|Z|/|Z_0|)/dt}{|Z|/|Z_0|} = \frac{k_{cat}}{K_m}[E_0] \quad (4)$$

The value of k_{cat}/K_m is referred to as "specificity constant" which is commonly used to represent the catalytic efficiency of enzymes. The value of -d(|Z|/|Z$_0$|)/dt of the modified REIS data can be calculated from the exponential fitting function |Z|/|Z$_0$| = 0.944·exp(-t/19.1) and plot vs. |Z|/|Z$_0$| in Fig. 6B. Clearly, the curve can be fit with a straight line with a slope 0.0522 s^{-1}. Since [E$_0$]=2.4 nM is known, the specificity constant k_{cat}/K_m can be derived as 2.17 x 10^7 $M^{-1}s^{-1}$. It is noteworthy that, despite the absolute impedance value |Z| varied in a large range on different NEA chips (from ~11,000 Ω to ~18,200 Ω in this study), the decay time constants derived from the normalized data (i.e. |Z|/|Z$_0$|) are very similar at the same PTP1B concentration. This is the critical quantity related to the enzyme activity.

In order to rigorously determine the specificity constant k_{cat}/K_m, we investigated the dephosphorylation reactions at two lower PTP1B concentrations at 1.8, and 1.2 nM. The representative kinetic curves of the normalized |Z|/|Z$_0$| at each PTP1B concentration are shown in Figs. S6A and S6C (Supplementary Information). Using the same method described above, the curves of -d(|Z|/|Z$_0$|)/dt vs. |Z|/|Z$_0$| can be derived and fit with straight lines as shown in Figs. S6B and S6D. Fig. 7A highlights three sets of data in 2.4, 1.8, and 1.2 nM PTP1B. A more comprehensive presentation containing 7 data sets was shown in Fig. S7 and summarized in Table 1. The slopes are clearly proportional to the enzyme concentration. The derived specificity constants k_{cat}/K_m are very close to each other with an average value at 2.13x10^7 $M^{-1}s^{-1}$ and a standard deviation of 0.91x10^5 $M^{-1}s^{-1}$. This value is consistent with the literature which lies between 1.1x10^6 $M^{-1}s^{-1}$ for human PTP1B to 2.9x10^7 $M^{-1}s^{-1}$ for rat PTP1 phosphatases [39, 40]. It is quite convincing that the electrochemical detection by REIS is a valid method for quantitative analyses of the PTP1B activity.

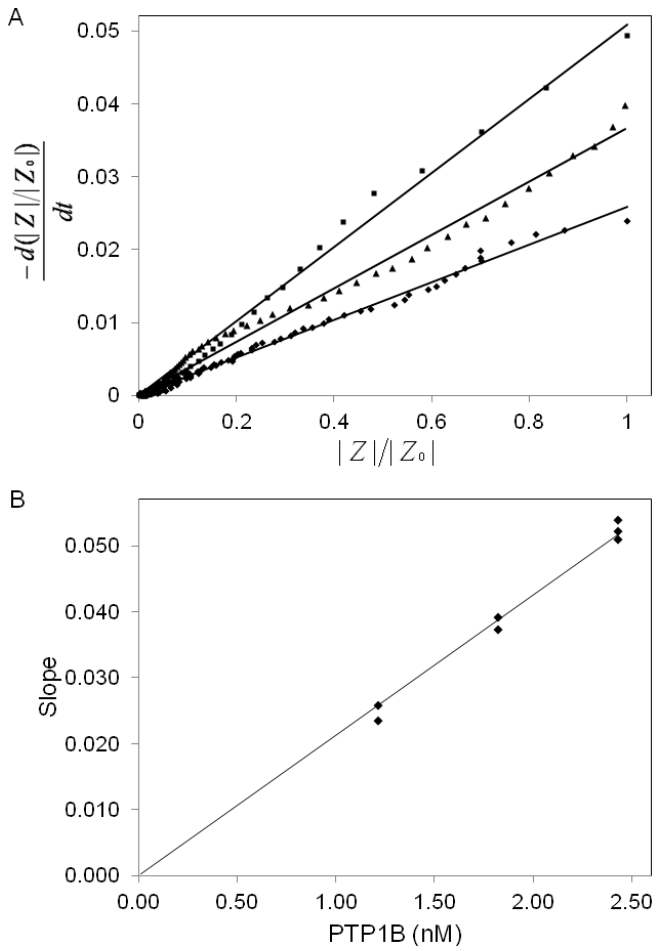

Fig. 7. Analyses of the enzymatic kinetics of the dephosphorylation process at three PTP1B concentrations. (A) The plot of $-d(|Z|/|Z_0|)/dt$ vs. $|Z|/|Z_0|$ fit with straight lines in 2.4 nM (■), 1.8 nM (▲), and 1.2 nM (♦) PTP1B, respectively. (B) The slopes of $-d(|Z|/|Z_0|)/dt$ vs. $|Z|/|Z_0|$ derived from 7 data sets at three PTP1B concentrations, clearly showing a linear relationship with the PTP1B concentration. The catalytic efficiency, k_{cat}/K_m, was calculated to be 2.13×10^7 $M^{-1}s^{-1}$ with a standard deviation of 9.1×10^5 $M^{-1}s^{-1}$.

In contrast to PTP1B, the reported specificity constant of c-Src kinase was two to three orders of magnitude lower, ranging from 2.4×10^3 to 2.5×10^4 $M^{-1}s^{-1}$ [35, 41-43]. This explains why we were not able to observe reliable kinetics with c-Src kinase. The small impedance change over much longer time can be easily overwhelmed by the baseline drift. For fast enzymatic reactions such as PTP1B

dephosphorylation, the potential of VACNF NEAs as a label-free electrochemical method can be fully utilized.

Table 1

Calculations of the catalytic efficiency k_{cat}/K_M of PTP1B dephosphorylation.

Sample	[PTP1B] (nM)	Slope of -d(|Z|/|Z$_0$|)/dt vs. |Z|/|Z$_0$| (s^{-1})	k_{cat}/K_m (x 10^7 $M^{-1}s^{-1}$)
1	2.43	0.0522	2.17
2	2.43	0.0509	2.12
3	2.43	0.0539	2.25
4	1.82	0.0373	2.07
5	1.82	0.0391	2.17
6	1.22	0.0235	1.96
7	1.22	0.0258	2.15

Note: The statistical value of k_{cat}/K_m is (2.13 ± 0.091) x 10^7 $M^{-1}s^{-1}$.

4. Conclusions

In summary, we have demonstrated the feasibility of a label-free electrochemical detection method for phosphorylation and dephosphorylation using peptide-functionalized VACNF NEAs by real-time impedance measurements. A peptide sequence specific to c-Src tyrosine kinase and PTP1B phosphatase was designed and validated with ELISA based protein tyrosine kinase assay. The peptide was functionalized to the surface of VACNF NEAs. Reversible phosphorylation and dephosphorylation upon adding c-Src kinase and PTP1B into the electrochemical cell were observed. The dephosphorylation reaction by PTP1B showed well-defined fast kinetics in REIS measurements, which can be quantitatively analyzed using Michaelis-Menten heterogeneous enzymatic model. Reliable specificity constant k_{cat}/K_m for PTP1B can be derived. In contrast, the signal during phosphorylation was limited by the slow

enzymatic kinetics. These results indicate the potential of the electrochemical impedance method, particularly when applied on nanoelectrode arrays, as a viable label-free method for profiling enzyme activities in fast reactions of specific peptide substrates.

Acknowledgment

This work was supported in part by grant number P20RR015563 from the National Center for Research Resources and by Award Number R15CA159250 from the National Cancer Institute. The content of this article is solely the responsibility of the authors and does not necessarily represent the official views of the NCI or the NIH.

References:

[1] P. Blume-Jensen, T. Hunter, Nature, 411 (2001) 355.

[2] T. Hunter, Cell, 100 (2000) 113.

[3] A.C. Dar, K.M. Shokat, Annual Review of Biochemistry, 80 (2011) 769.

[4] J.L. McConnell, B.E. Wadzinski, Molecular Pharmacology, 75 (2009) 1249.

[5] L.M. Scott, H.R. Lawrence, S.M. Sebti, N.J. Lawrence, J. Wu, Current Pharmaceutical Design, 16 (2010) 1843.

[6] P. Cohen, Nat Rev Drug Discov, 1 (2002) 309.

[7] B.T. Houseman, J.H. Huh, S.J. Kron, M. Mrksich, Nat Biotech, 20 (2002) 270.

[8] B.E. Turk, J.E. Hutti, L.C. Cantley, Nat. Protocols, 1 (2006) 375.

[9] C.J. Hastie, H.J. McLauchlan, P. Cohen, Nat. Protocols, 1 (2006) 968.

[10] O. von Ahsen, U. Bömer, ChemBioChem, 6 (2005) 481.

[11] M. Sato, T. Ozawa, K. Inukai, T. Asano, Y. Umezawa, Nat Biotech, 20 (2002) 287.

[12] Y. Umezawa, Biosensors and Bioelectronics, 20 (2005) 2504.

[13] K.-y. Tomizaki, H. Mihara, Molecular BioSystems, 2 (2006) 580.

[14] M.D. Allen, L.M. DiPilato, M. Rahdar, Y.R. Ren, C. Chong, J.O. Liu, J. Zhang, ACS Chemical Biology, 1 (2006) 371.

[15] X. Han, S. Shigaki, T. Yamaji, G. Yamanouchi, T. Mori, T. Niidome, Y. Katayama, Analytical Biochemistry, 372 (2008) 106.

[16] H. Steen, J.A. Jebanathirajah, M. Springer, M.W. Kirschner, Proc. Nat. Aca. Sci. USA, 102 (2005) 3948.

[17] R. Kr??ger, D. K??bler, R. Palliss??, A. Burkovski, W.D. Lehmann, Analytical Chemistry, 78 (2006) 1987.

[18] L.G. F?gerstam, s. Frostell-Karlsson, R. Karlsson, B.r. Persson, I. R??nnberg, Journal of Chromatography A, 597 (1992) 397.

[19] P. Stenlund, A. Frostell-Karlsson, O.P. Karlsson, Analytical Biochemistry, 353 (2006) 217.

[20] B. Catimel, M. Layton, N. Church, J. Ross, M. Condron, M. Faux, R.J. Simpson, A.W. Burgess, E.C. Nice, Analytical Biochemistry, 357 (2006) 277.

[21] K. Viht, S. Schweinsberg, M. Lust, A. Vaasa, G. Raidaru, D. Lavogina, A. Uri, F.W. Herberg, Analytical Biochemistry, 362 (2007) 268.

[22] D.M. Rothman, M.D. Shults, B. Imperiali, Trends in Cell Biology, 15 (2005) 502.

[23] K. Kerman, H. Song, J.S. Duncan, D.W. Litchfield, H.-B. Kraatz, Anal. Chem., 80 (2008) 9395.

[24] K. Kerman, H.-B. Kraatz, Biosensors and Bioelectronics, 24 (2009) 1484.

[25] T.J. Yeatman, Nat Rev Cancer, 4 (2004) 470.

[26] R.B. Irby, T.J. Yeatman, Oncogene, 19 (2000) 5636.

[27] L.C. Kim, L.X. Song, E.B. Haura, Nature Reviews Clinical Oncology, 6 (2009) 587.

[28] S.-C. Yip, S. Saha, J. Chernoff, Trends in Biochemical Sciences, 35 (2010) 442.

[29] A. Ostman, C. Hellberg, F.D. Bohmer, Nat Rev Cancer, 6 (2006) 307.

[30] L. Lessard, M. Stuible, M.L. Tremblay, Biochimica et Biophysica Acta (BBA) - Proteins & Proteomics, 1804 (2010) 613.

[31] J. Li, J.E. Koehne, A.M. Cassell, H. Chen, H.T. Ng, Q. Ye, W. Fan, J. Han, M. Meyyappan, Electroanalysis, 17 (2005) 15.

[32] J. Li, H.T. Ng, A. Cassell, W. Fan, H. Chen, Q. Ye, J. Koehne, J. Han, M. Meyyappan, Nano Letters, 3 (2003) 597.

[33] J. Koehne, H. Chen, J. Li, A.M. Cassell, Q. Ye, H.T. Ng, J. Han, M. Meyyappan, Nanotechnology, 14 (2003) 1239.

[34] J.E. Koehne, H. Chen, A.M. Cassell, Q. Ye, J. Han, M. Meyyappan, J. Li, Clin Chem, 50 (2004) 1886.

[35] T.M. Johnson, J.W. Perich, J.D. Bjorge, D.J. Fujita, H.-C. Cheng, The Journal of Peptide Research, 50 (1997) 365.

[36] A.V. Melechko, V.I. Merkulov, T.E. McKnight, M.A. Guillorn, K.L. Klein, D.H. Lowndes, M.L. Simpson, J. Appl. Phys., 97 (2005) 41301.

[37] E. Katz, I. Willner, Electroanalysis, 15 (2003) 913.

[38] O.A. Gutierrez, M. Chavez, E. Lissi, Analytical Chemistry, 76 (2004) 2664.

[39] A. Salmeen, J.N. Andersen, M.P. Myers, N.K. Tonks, D. Barford, Molecular Cell, 6 (2000) 1401.

[40] Z.Y. Zhang, D. Maclean, D.J. McNamara, T.K. Sawyer, J.E. Dixon, Biochemistry, 33 (1994) 2285.

[41] P.A. Cole, P. Burn, B. Takacs, C.T. Walsh, Journal of Biological Chemistry, 269 (1994) 30880.

[42] Y. Liu, K. Shah, F. Yang, L. Witucki, K.M. Shokat, Chemistry & Biology, 5 (1998) 91.

[43] J. Shaffer, G.Q. Sun, J.A. Adams, Biochemistry, 40 (2001) 11149.

Label-free electrochemical impedance detection of kinase and phosphatase activities using carbon nanofiber nanoelectrode arrays

Yifen Li[1], Lateef Syed[1], Jianwei Liu[1], Duy Hua[1], Jun Li[1,*]

[1]Department of Chemistry, Kansas State University, Manhattan, KS 66506, USA

Supporting Information

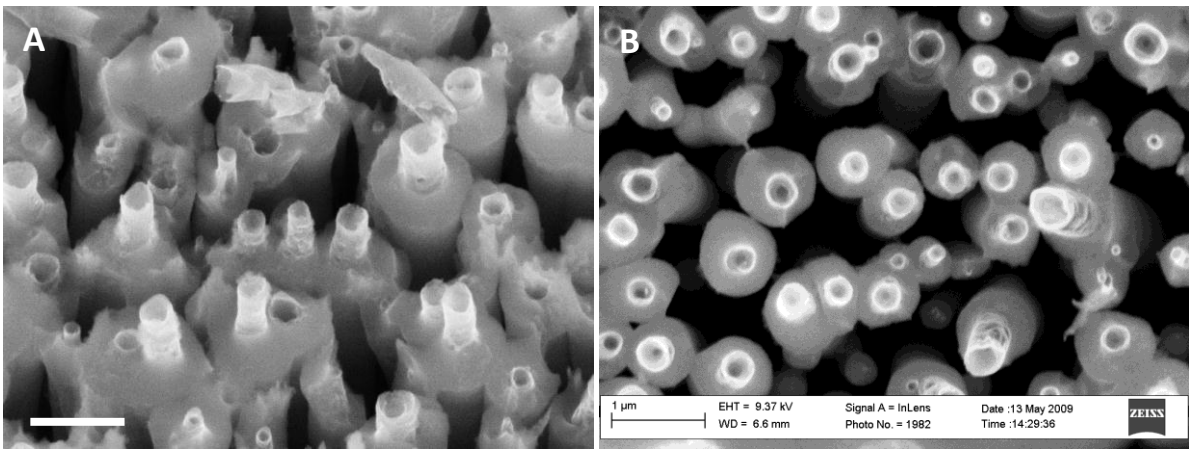

Fig. S1. Field-emission scanning electron micriscopic images of vertically aligned carbon nanofiber nanoelectrode arrays at 30° perspective view (A) and topview (B). The scale bars are 1 μm. Note: This sample was over-etched with reactive ion etching (RIE) so that clearer images of the carbon nanofiber tip can be observed.

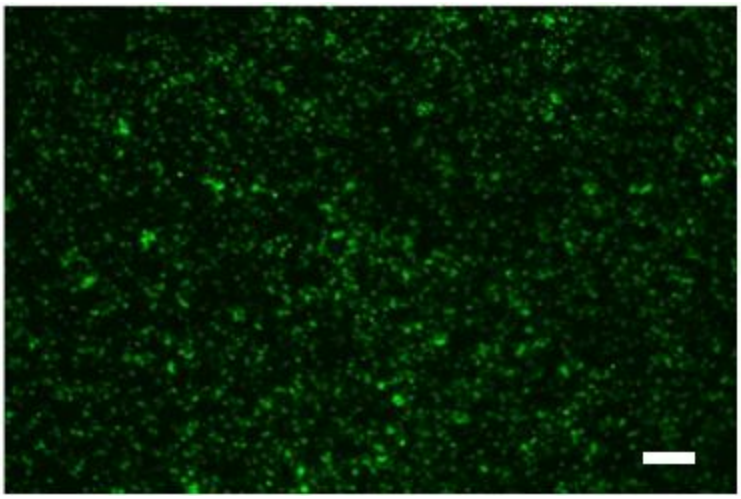

Fig. S2. The fluorescence image over the VACNF NEA chip showing streptavidin-labelled yellow-green fluorescent beads. The scale bar is 20 μm.

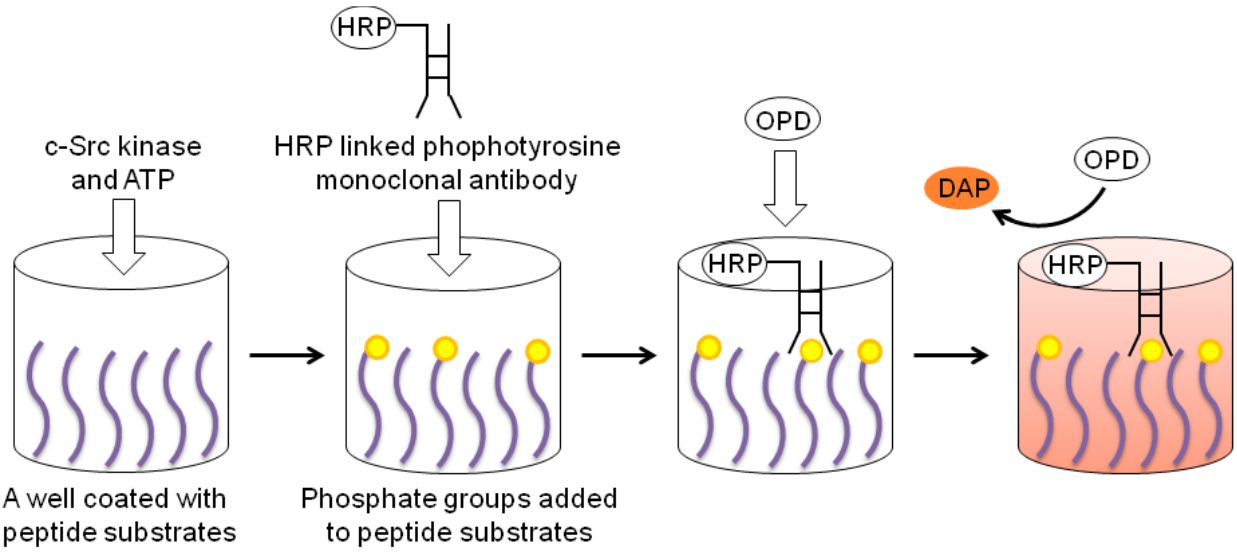

Fig. S3. The procedure of the ELISA assay to validate phosphorylation and dephosphorylation. The peptide substrates was first coated on the surface of 96-wellplate by incubating the peptide solution in the well at 37 °C overnight. After rinsing and dring at 37 °C for 2 hours, the solution containing c-Src kinase and ATP was added to the well and incubated for 30 minutes at room temperature. The wells were rinsed and refilled with the solution containing a horseradish peroxidase (HRP) linked phosphotyrosine monoclonal antibody and incubated for 30

minutes at room temperature. After rinsing off the unbound antibody, a freshly prepared *o*-phenylenediamine (OPD) solution was added. HRP catalyzed the conversion of colorless OPD into brown-color 2,3-diaminophenazine (DAP) which has strong molar absorptivity at 490 nm wavelength. The absorbance at 490 nm was finally read by a microplate reader.

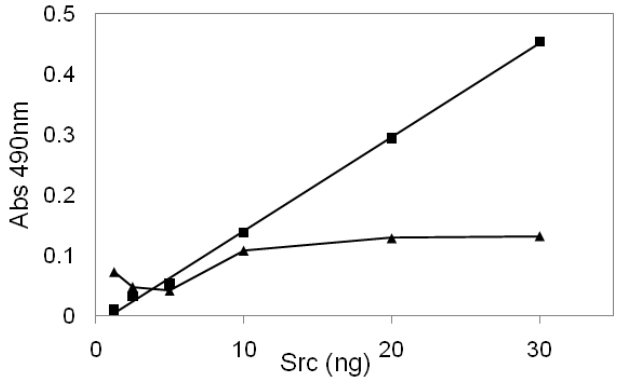

Fig. S4. The effects of $K_3Fe(CN)_6$/$K_4Fe(CN)_6$ mediators on the activity of c-Src kinase (61.7 kDa) in phosphorylation of biotinylated peptides by the ELISA assay. The squares (■) represent the measurements in the commercial tyrosine kinase buffer (500 mM HEPES, pH 7.4, 200 mM $MgCl_2$, 1 mM $MnCl_2$, and 2 mM Na_3VO_4) and the triangles (▲) are the results in the tyrosine kinase buffer after addition of 1 mM $K_3Fe(CN)_6$ and 1 mM $K_4Fe(CN)_6$. The concentration of ATP was fixed at 0.3 mM in all measurements. The absorbance at 490 nm corresponds to the amount of phosphorylated tyrosine, which is proportional to the concentration of c-Src kinase at the concentration varying from 0.18 nM to 5.9 nM (1.25-40 ng in 110 μL).

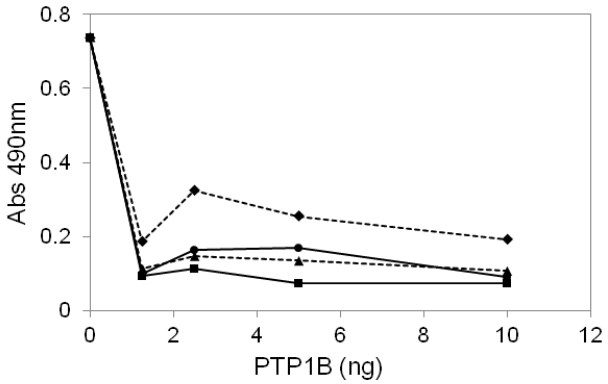

Fig. S5. The effects of $K_3Fe(CN)_6/K_4Fe(CN)_6$ mediators and buffer composition on the activity of PTP1B phosphatase (37.4 kDa) by the ELISA assay. The buffer solutions are: (■) the commercial protein tyrosine phosphatase (PTP) buffer (50 mM HEPEs, pH 7.2, 1 mM EDTA, 1 mM DTT, and 0.05% NP-40); (▲) the commercial PTP buffer plus 1 mM $K_3Fe(CN)_6$ and 1 mM $K_4Fe(CN)_6$; (●) the modified PTP buffer (with NP-40 removed); and (♦) the modified PTP buffer plus 1 mM $K_3Fe(CN)_6$ and 1 mM $K_4Fe(CN)_6$. The plate was coated with the biotinylated peptide whose tyrosine residue was phosphorylated by incubating in 5.9 nM of c-Src kinase for 1 hour before this experiment. The PTP1B phosphatase concentration was varied from 0.30 nM to 2.4 nM (1.25-10 ng in 110 μL). Removal of the phosphate group from the phosphorylated tyrosine residue, i.e. dephosphorylation, caused the absorbance at 490 nm to drop. The decrease amplitude indicated the PTP1B activity.

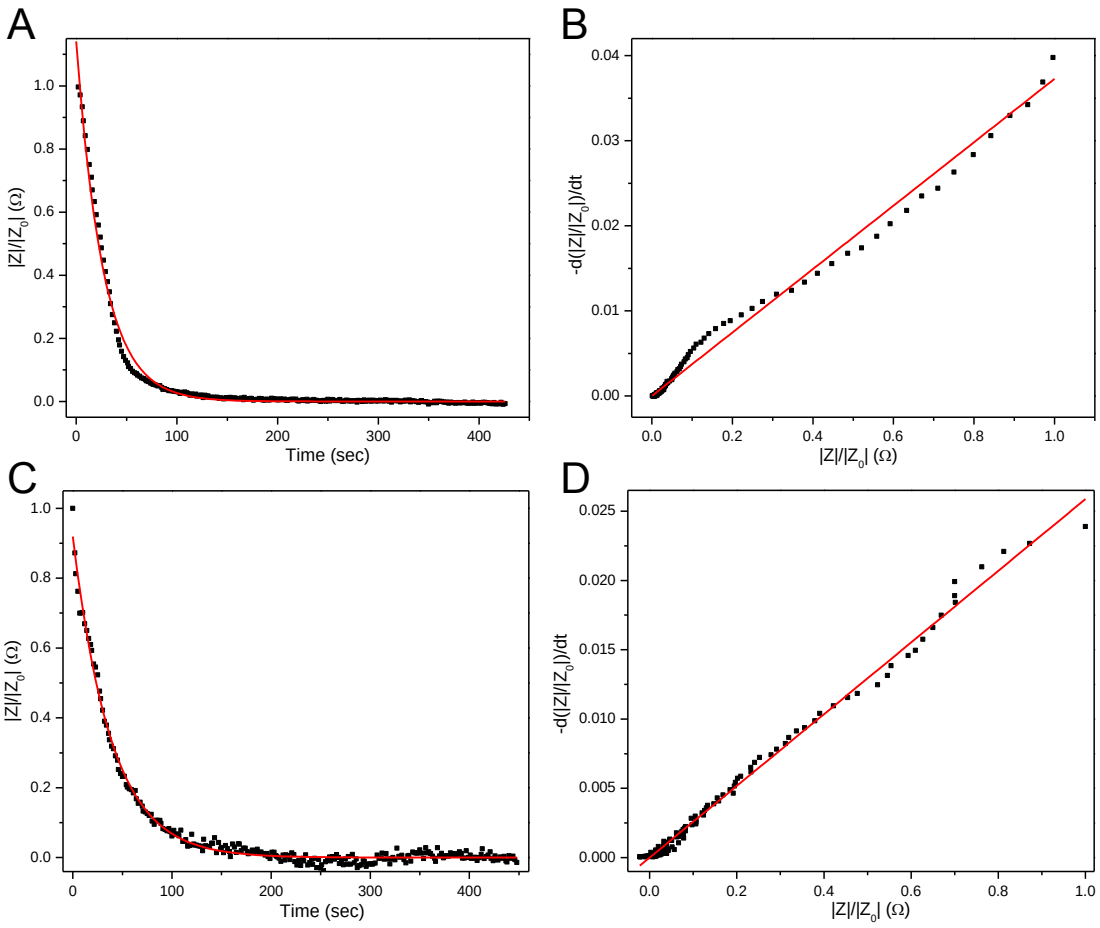

Fig. S6. Analyses of the enzymatic kinetics of the dephosphorylation in (A,B) 1.8 nM PTP1B (7.5 ng in 110 μL solution) and (C,D)1.2 nM PTP1B (5.0 ng in 110 μL solution). (A) The normalized real-time impedance data fit with an exponential function $|Z|/|Z_0| = 1.14 \cdot \exp(-t/26.6)$. (B) The curve of $-d(|Z||Z_0|)/dt$ vs. $|Z|/|Z_0|$ fit with a straight line giving a slope 0.0373 s^{-1}. (C) The normalized real-time impedance data fit with an exponential function $|Z|/|Z_0| = 0.919 \cdot \exp(-t/38.5)$. (D) The curve of $-d(|Z||Z_0|)/dt$ vs. $|Z|/|Z_0|$ fit with a straight line giving a slope 0.0258 s^{-1}.

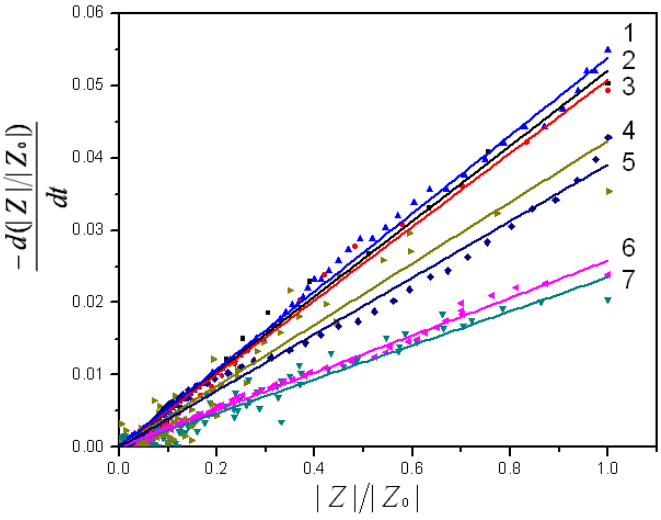

Fig. S7. Analyses of the enzymatic kinetics for the dephosphorylation at three different PTP1B concentrations: 2.4 nM - Sample No. 1-3; 1.8 nM - Sample No. 4 and 5; 1.2 nM - Sample No. 6 and 7. The slope of $-d(|Z|/|Z_0|)/dt$ vs. $|Z|/|Z_0|$ is clearly proportional to the PTP1B concentration.